

Ascl1 and Ngn2 convert mouse embryonic stem cells to neurons via functionally distinct paths

Received: 11 July 2022

Accepted: 9 August 2023

Published online: 02 September 2023

 Check for updates

Gintautas Vainorius^{1,2} ✉, Maria Novatchkova^{1,3}, Georg Michlits^{1,2,5},
Juliane Christina Baar¹, Cecilia Raupach¹, Joonsun Lee^{1,2},
Ramesh Yelagandula^{1,6}, Marius Wernig⁴ & Ulrich Elling¹ ✉

Ascl1 and Ngn2, closely related proneural transcription factors, are able to convert mouse embryonic stem cells into induced neurons. Despite their similarities, these factors elicit only partially overlapping transcriptional programs, and it remains unknown whether cells are converted via distinct mechanisms. Here we show that Ascl1 and Ngn2 induce mutually exclusive side populations by binding and activating distinct lineage drivers. Furthermore, Ascl1 rapidly dismantles the pluripotency network and installs neuronal and trophoblast cell fates, while Ngn2 generates a neural stem cell-like intermediate supported by incomplete shutdown of the pluripotency network. Using CRISPR-Cas9 knockout screening, we find that Ascl1 relies more on factors regulating pluripotency and the cell cycle, such as Tcf7l1. In the absence of Tcf7l1, Ascl1 still represses core pluripotency genes but fails to exit the cell cycle. However, overexpression of Cdkn1c induces cell cycle exit and restores the generation of neurons. These findings highlight that cell type conversion can occur through two distinct mechanistic paths, even when induced by closely related transcription factors.

Cell identity in development is typically crafted by an interplay of multiple transcriptional activators and inhibitors successively restricting the lineage. Cells gradually rewire their gene transcriptional network, retarget multiple transcriptional factors to new loci, reshape their epigenetic landscape, and establish epigenetic barriers to lock the next developmental state^{1–5}. In contrast, directed lineage conversions rely on the expression of transcription factors (TF) in alien cellular contexts that can be affected by different distributions of epigenetic marks^{6,7}, posttranslational modifications^{8,9}, interaction partners^{10–13}, and other factors^{14,15}. This can affect the binding and activity of the TF. Conflicting or incomplete cues of lineage formation

allow the formation of alternative lineages during directed lineage conversion regimes^{16–19}. These conversions do not necessarily follow developmental trajectories, and can also skip intermediate cell states^{20,21}. As such, they provide an opportunity to study alternative inroads to cell states. Thus, cellular reprogramming can be used as a powerful tool to address fundamental principles underlying lineage specifications and generate models for a study of various diseases as well as potential therapeutic modalities^{22,23}.

Basic helix loop helix (bHLH) TFs have proven to be efficient factors for lineage conversion. Various proneural factors, such as Ascl1, Ngn1, Ngn2, Neurod1 and Neurod4 have been utilized to convert

¹Institute of Molecular Biotechnology of the Austrian Academy of Science (IMBA), Dr. Bohr-Gasse 3, Vienna BioCenter (VBC), 1030 Vienna, Austria. ²Vienna BioCenter PhD Program, a Doctoral School of the University of Vienna and Medical University of Vienna, A-1030 Vienna, Austria. ³Research Institute of Molecular Pathology (IMP), Campus-Vienna-BioCenter 1, Vienna BioCenter (VBC), 1030 Vienna, Austria. ⁴Institute for Stem Cell Biology and Regenerative Medicine, Department of Pathology, Stanford University, Stanford, CA, USA. ⁵Present address: JLP Health GmbH, Himmelhofgasse 62, 1130 Vienna, Austria. ⁶Present address: Laboratory of Epigenetics, Cell Fate & Disease, Centre for DNA Fingerprinting and Diagnostics (CDFD), Uppal, Hyderabad 500039, India.

✉ e-mail: gintautas.vainorius@imba.oeaw.ac.at; ulrich.elling@imba.oeaw.ac.at

different cell types to functioning neurons^{24–28}. Among those, *Ascl1* and *Ngn2* (encoded by the *Neurog2* gene) have emerged as preferred tools for in vitro neuronal reprogramming²⁴. Both are master regulators of neuronal fate in the developing central nervous system. Expression of *Ascl1* in ventral telencephalon progenitor cells generates inhibitory GABAergic interneurons, whereas *Ngn2* directs dorsally situated progenitors toward excitatory neurons with glutamatergic identity. Although, *Ascl1* and *Ngn2* give rise to different subtypes in the telencephalon, expression of *Ngn2* in the ventral telencephalon can rescue *Ascl1* null mice²⁹. Interestingly, while expression of *Ascl1* and *Ngn2* in astrocytes can recapitulate developmental neuronal subtype specification to GABAergic or glutamatergic neurons, respectively, expression of *Ascl1* in mouse embryonic fibroblasts (MEF), as well as expression of *Ascl1* or *Ngn2* in mouse embryonic stem cells (ESC), lead to primarily glutamatergic neurons^{27,28,30}. Thus, the subtype specification depends on the initial cell type. It is thus vital to understand how ectopically expressed TFs interact with the initial cellular context to define the outcome of conversions.

The ability to transition toward the same states using different transcription factors gives an opportunity to directly contrast differentiation mechanisms. In an elegant study, Aydin et al. showed that *Ascl1* and *Ngn2* in ESC prefer binding distinct E-box motifs⁶. This, in turn, initiates different accessibility and gene expression patterns, influencing downstream TFs, while still resulting in the formation of glutamatergic induced neurons (iN) in both cases^{6,27,28,30}. However, downstream mechanistic differences, such as the downregulation of the initial pluripotency network, are still not understood. Furthermore, even though *Ascl1* and *Ngn2* possess ‘pioneering’ TF properties, their binding and expression can be influenced by cellular context, e.g., *Ascl1* binds and induces muscle lineage when expressed in MEF, but myoblast induction was not reported in ESC^{6,16,19}.

In this work, we study the mechanistic differences in how the expression of *Ascl1* or *Ngn2* transitions cells between two identical states. We observe different side lineages forming in parallel to neurons due to differential binding and different strategies for exiting pluripotency upon *Ascl1* and *Ngn2* induction: *Ascl1* rapidly shuts down the pluripotency network and arrests the cell cycle to install neuronal or trophoblast states, while *Ngn2* retains *Sox2* expression to produce neuron stem cells (NSC). CRISPR/Cas9 forward genetic screens revealed that genes involved in pluripotency regulation and cell cycle control are affecting neuronal reprogramming by *Ascl1*, but not *Ngn2*. Our results highlight different mechanistic pathways to iN employed by these bHLH TFs.

Results

Ascl1 and *Ngn2* convert ESC to iN but generate different side lineages

Ectopic expression of *Ascl1* or *Ngn2* in mouse embryonic stem cells (ESCs) is sufficient to induce terminal differentiation into neurons²⁸. Yet, the differences in transition mechanism toward neurons as well as possible side populations are not well characterized^{16,31}. To examine this cell type conversion in detail, we generated clonal ESC cell lines expressing rtTA and TetO-*Ascl1* or TetO-*Ngn2*^{27,28} (Supplementary Fig. 1a). After doxycycline (Dox) addition, ESCs are rapidly converted to induced neurons: *Ascl1* and *Ngn2* produce cells expressing the neuronal marker TUBB3 and displaying neuronal morphology from day 3 and day 2 onward, respectively (Supplementary Fig. 1a). To report neuronal fate in these cell lines we endogenously tagged the pan-neuronal marker gene *Mapt* on its C-terminus with the fluorescent protein Venus²⁷ (Supplementary Fig. 1b) and performed time-resolved bulk RNAseq upon Dox-induction. Cells were sorted into Venus-positive neurons and Venus-negative cell populations (Fig. 1a) from day 3 onward. As reported before^{28,30}, both *Ascl1* and *Ngn2* give rise to similar iN cell identities (Fig. 1b; Supplementary Fig. 1c–e). Thus, initial ESC and terminal iN states are very similar between *Ascl1* and *Ngn2*-

induced conversions (Supplementary Fig. 1b bottom). This is in line with previous observations that transcriptomes converge to drive iN formation despite differences in the initial transcriptional response⁶ and follow an overall similar trajectory between ESC and iN in the PCA analysis (Fig. 1c, d; Supplementary Fig. 1g).

To investigate cells that fail to make iN in more detail, we focused on the *Mapt*-Venus-negative cells, which could represent incomplete or alternative differentiation outcomes. *Mapt*-Venus-negative cells generated by *Ascl1* cluster closer to the initial ESC populations in PCA plots than *Ngn2*-induced *Mapt*-negative cells (Fig. 1c). However, this is not due to retaining a population of undifferentiated ESC as only a marginal number of cells express ESC marker NANOG in terminal population (Supplementary Fig. 1g), and NANOG and OCT4 are not expressed in *Mapt*-Venus population (Supplementary Fig. 1h). To identify the alternative type of cells generated by *Ascl1*, we used PanglaoDB³² using genes differentially expressed between Venus-negative and positive populations at day 6 (Fig. 1e, f; Supplementary Fig. 2a). Interestingly, *Ascl1* produce cells expressing trophoblast markers such as *Hand1*, *Cdx2*, *Tpbpa*, *Krt8* (Fig. 1e, g; Supplementary Fig. 2b–g) with mesenchymal morphology, which were not present in *Ngn2*-induced cultures (Fig. 1g, Supplementary Fig. 2b, c, f). We termed these cells induced-Trophoblast-like-cells (iT). Interestingly, many of the *Krt8*, *Cdx2* positive iTs appeared binucleated, which could be a result of multinucleation similar to trophoblast lineage development in vivo (Supplementary Fig. 2e)³³. The induction of iT could be due to *Ascl1* mimicking the bHLH transcription factor *Ascl2*, a driver for the trophoblast lineage. Both *Ascl1* and *Ascl2* are evolutionary close and share near identical DNA binding domains and bind similar E-box motifs (Supplementary Fig. 2h–k)^{33–37}. Lastly, to exclude clonal effects of the cell line used, we repeated these experiments in the background of an alternative mouse ESC line, E14. We introduced rtTA via a piggybac transposon vector and expressed *Ascl1* from a Dox-inducible viral vector²⁷ and generated 24 single-cell derived clones. All the clones showed the formation of both iN and iT, suggesting that the formation of iTs is a reproducible side product of ectopic *Ascl1* expression in mouse ESCs (Supplementary Fig. 3).

In contrast to *Ascl1* induction, *Ngn2* induces *Mapt*-negative cells expressing NSC markers, such as *Sox2*, *Pax3*, *Pax6*, *Nes* (Fig. 1f, h; Supplementary Fig. 2a, 4a, b), as previously described^{21,38}. Furthermore, *Ngn2* reprogramming could be locked in the NSC-like state (iNSC) in the presence of FGF2 and EGF and is dependent on the Notch pathway^{39,40} (Supplementary Fig. 4c, d). In contrast, we did not observe NSC markers upregulated during *Ascl1*-induced differentiation (Fig. 1h, Supplementary Fig. 4b, c). To see if *Ngn2* can use iNSC state as proliferative intermediate, we differentiated cells in the presence or absence of cytosine β-D-arabinofuranoside (AraC) from day 4 post-induction to inactivate dividing cells (Supplementary Fig. 4e). Indeed, addition of AraC drastically reduces *Ngn2*-produced iNs, while *Ascl1* was insensitive to AraC treatment, suggesting that no continuously proliferative intermediate is present during *Ascl1*-induced iN reprogramming (Supplementary Fig. 4e). In summary, despite *Ascl1* and *Ngn2* converting mESC to similar iN subtypes, *Ascl1* and *Ngn2* produce distinct additional alternative cell lineages, suggesting that despite identical initial and terminal populations, differences exist that we sought to understand further (Supplementary Fig. 1b bottom).

Ascl1 and *Ngn2* initiate paths with different transcriptional programs

To get a better understanding of different transcriptional response invoked by *Ascl1* and *Ngn2*, we performed bulk RNAseq and ChIPseq upon day 1 (Fig. 1a). Both *Ascl1* and *Ngn2* induce general neuronal markers such as *Tubb3*, *Map2* and *Oncut2* and downregulate general pluripotency markers like *Nanog*, *Klf4* (Fig. 1i). Furthermore, *Ascl1*-strongly induces downstream targets *Tfap2b*, *Lmx1b*, while

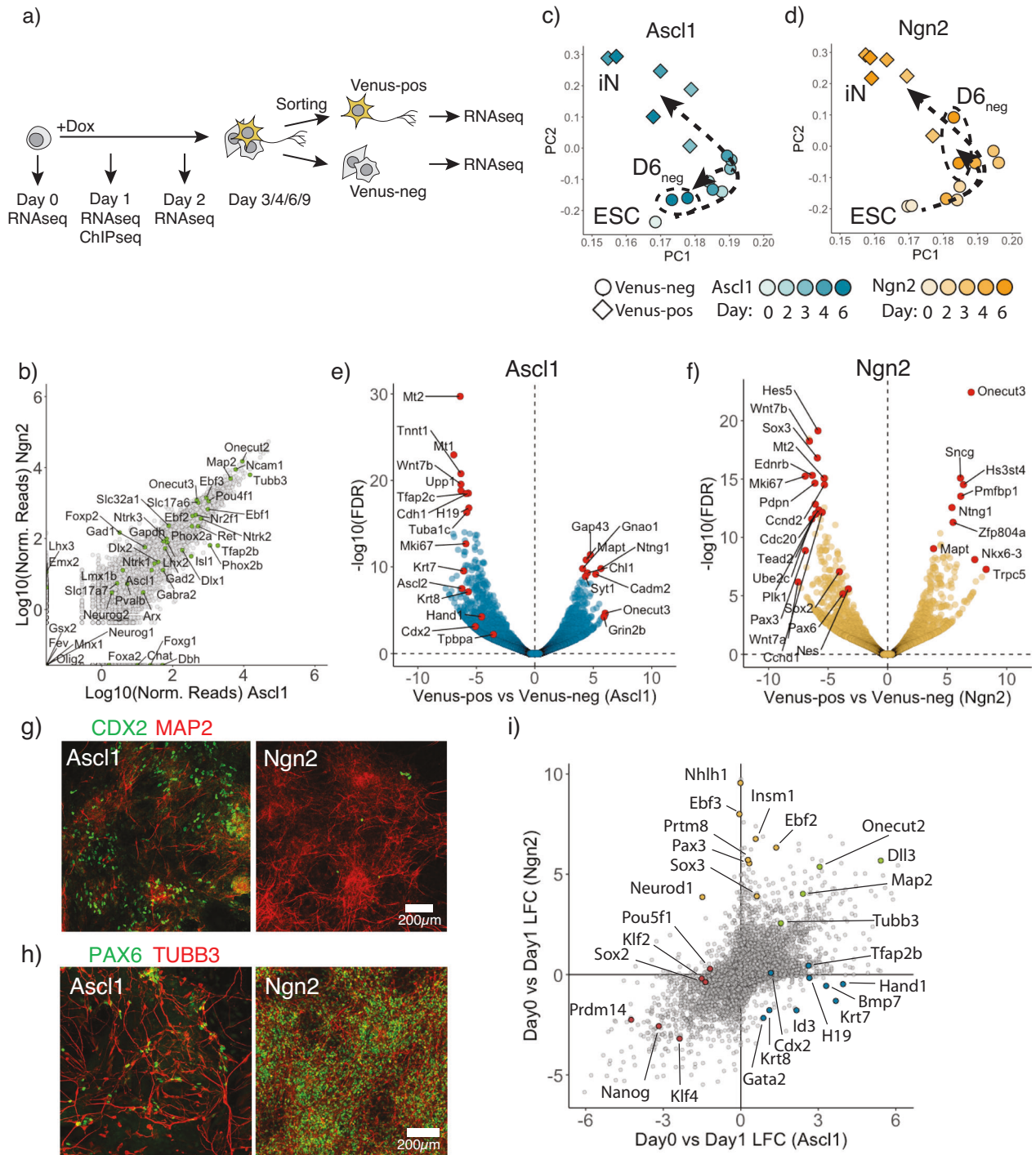


Fig. 1 | Ascl1 and Ngn2 induce different alternative lineages. **a** Schematic overview of the experimental design. **b** Scatter plot comparing gene expression at Day 6 between Ascl1 and Ngn2 Venus-positive cells with various neuronal subtype specific markers indicated in green. **c, d** Principal component analysis of time-resolved bulk RNAseq after Ascl1 (**c**) or Ngn2 (**d**). Each data point corresponds to the single time point replicate. Color intensity shows day post-induction. Shape corresponds the Mapt-Venus reporter upregulation. Arrows show the trajectory cells take after the Ascl1 (**c**) or Ngn2 induction (**d**). **e, f** Volcano plot comparing gene expression between Venus-positive and negative populations at day 6 post-induction of Ascl1 (**e**) or Ngn2 (**f**). Red circles denote top significantly upregulated or downregulated genes as well as example genes marking in trophoblast (**e**) or NSC lineages (**f**).

g Representative immunostained cells for a trophoblast marker CDX2 and a neuronal marker Map2 at day 6 post-induction of Ascl1 or Ngn2. Trophoblast markers were expressed only after Ascl1 induction, but not Ngn2. **h** Representative immunostained cells for an NSC marker PAX6 and a neuronal marker TUBB3 at day 6 post-induction of Ascl1 or Ngn2. NSC markers were expressed only after Ngn2 expression, but not Ascl1. **i** Scatter plot comparing gene expression changes between Ascl1 and Ngn2 at day 1 post-induction. Highlighted circles are example genes that are neuronal markers expressed in both (green), trophoblast Ascl1 specific markers (blue), NSC Ngn2 specific markers (yellow), pluripotency related genes (red). Source data are provided as a Source Data file.

Ngn2 strongly upregulates *Neurod1*, *Nhlh1* (Fig. 1i). In addition, Ascl1 upregulate Trophoblast lineage markers, e.g., *Krt7/8*, *Hand1*, while Ngn2 upregulates expression of NSC related genes, like *Pax3* and *Sox3* (Fig. 1i). Interestingly we observed that early in reprogramming cells are positive for both—neuronal and trophoblast markers (Supplementary Fig. 5a, b). In addition, we reanalyzed available scRNAseq data⁶ for Day 2 of ESC to iN conversion by Ascl1 and Ngn2 and could also observe cells positive for both neuronal and trophoblast markers (Supplementary Fig. 5c, d). This suggests that Ascl1 can induce both lineages simultaneously, which later are resolved into iN or iT cells (Supplementary Fig. 5b).

As reported by Aydin and colleagues⁶, Ascl1 and Ngn2 show different preferences for E-box motives, which in turn result in the activation of different subset of genes. Indeed, we confirmed Ascl1 and Ngn2 differential binding in ESC (Supplementary Fig. 6a). Furthermore, we see that Ascl1 and Ngn2 target genes differentially expressed between them as well as genes involved in the different alternative lineages, e.g., *Hand1*, *Cdx2*, *Krt8* or *Neurod1*, *Pax3*, respectively (Supplementary Fig. 6b). Interestingly, Ascl1 binds trophoblast related genes also in MEF, although without iT induction (Supplementary Fig. 7a, b). However, in addition to iN induction, Ascl1 overexpression in MEF leads to Ascl1 binding to the skeletal muscle genes and the induction of myocytes^{7,16}. Indeed, in ESC Ascl1 also strongly bind to skeletal muscle lineage-related genes, e.g., *Myod1*, *Myog*, *Myf3*, *Tnnt2* (Supplementary Fig. 7c). However, we did not observe upregulation of these genes (Supplementary Fig. 7d). Thus, it is tempting to speculate that cellular context, such as cell type-specific histone modifications or transcription factors, affects the choice of the alternative lineage induced. Thus, in addition to the induction of the neuronal transcriptional program, additional genes are bound and transcribed, leading to the formation of alternative lineages. This “off target” transcriptional program depends on overexpression of transgene, e.g., Ascl1 or Ngn2, as well as the cellular context, e.g., ESC or MEF.

To investigate the general principles of the early transcriptional response in more depth, we used the STRING database to examine the gene regulatory network (GRN) of Ascl1 and Ngn2-upregulated differentially expressed genes (DEGs) one day after induction (Supplementary Fig. 8a, b). Both Ascl1 and Ngn2 DEGs form networks containing three distinct gene groups. Interestingly, Ascl1 and Ngn2 GRNs share groups containing genes involved in RNA and sterol metabolism, which can be attributed to the metabolic shift during conversion^{41,42}. Furthermore, Ngn2 forms a more interconnected network than Ascl1, suggesting that Ngn2 invokes a more coherent transcriptional response than Ascl1 (Supplementary Fig. 8c).

To analyze the differences in more detail, we looked at the central-most connected nodes of both GRNs (Supplementary Fig. 8d, e). In contrast to Ascl1, Ngn2 induce genes driving neuronal differentiation *Neurog2*, *Neurod1*, *Neurog1*, *Lhx2/3*, *Otx2*, as well as genes involved in neural stem cell differentiation: *Notch1*, *Hes5*, *Pax3*, centering GRN around them (Supplementary Fig. 8e–g). Interestingly, Ngn2, *Neurod1* and Ngn2 are known to be able to convert ESC to iN⁴³. Thus, such a positive feedback loop together with the induction of strong lineage drivers and highly interconnected GRN can allow a more robust iN conversion and faster independence from the initial induction of the cassette. To test this hypothesis, we induced cells for 2, 4, or 6 days (Supplementary Fig. 8h). Indeed, we observe that efficient iN conversion with Ascl1 relies on the sustained expression of Ascl1, while Ngn2 efficiently induces conversion already after 2 days of induction (Supplementary Fig. 8h).

In summary, Ascl1 and Ngn2 bind and invoke different transcriptional profiles and subsequent mechanistic differences of the ESC to iN conversion. Where Ascl1 induction relies on the sustained expression of Ascl1, Ngn2 induces an overall more coherent network allowing efficient and fast reprogramming as well as induction of a proliferative intermediate.

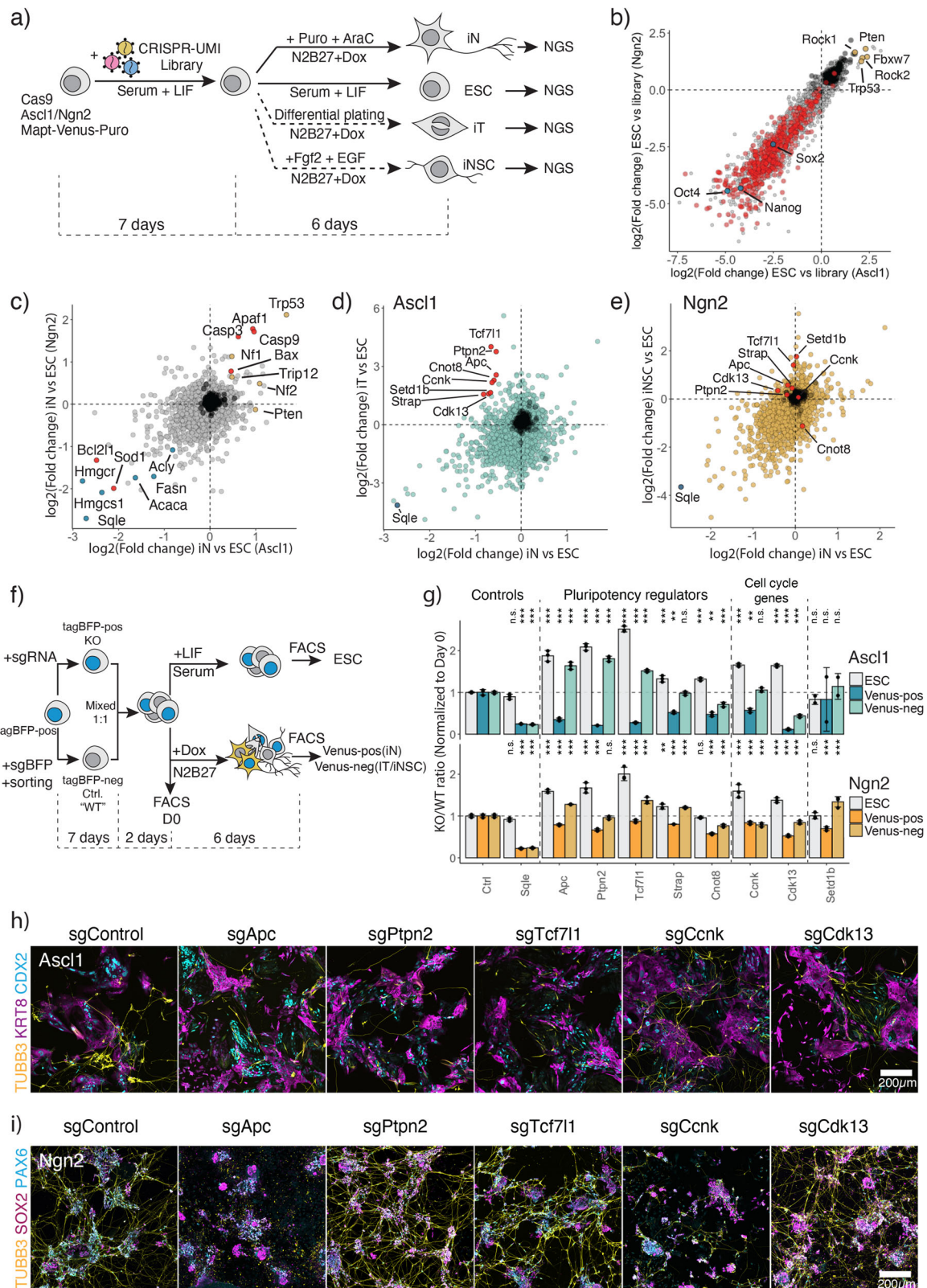
Loss-of-function CRISPR/Cas9 screen to identify genetic dependencies for ESC to iN conversion

To establish a mechanistic handle on the underlying differences between Ascl1- and Ngn2-induced ESC reprogramming, we performed a CRISPR/Cas9 loss-of-function screen. We aimed to investigate two aspects of this conversion: first, the genetic dependencies of Ascl1 and Ngn2-induced neuronal conversion, and second, to elucidate the genes involved in alternative state formation (Fig. 2a). For this, ESC were infected with retroviral CRISPR-UMI sgRNA library containing ~27,000 guides targeting 6630 genes (4 guides per gene) and 108 non-targeting guides⁴⁴. We then differentiated ESC for 6 days and enriched for iN using AraC and puromycin treatment (Fig. 2a, Supplementary Fig. 1b, 9a). In addition, we assessed dependencies for iT and iNSC differentiation (Fig. 2a, see “Methods”). For an initial assessment of the screening results, we compared the depletion of known essentials in ESC versus the Library (Fig. 2b). We indeed observed a strong depletion in common essential genes as defined by Hart et al.⁴⁵. Furthermore, genes at the core pluripotency network (*Nanog*, *Sox2*, *Pou5f1*) are among the most essential genes, while tumor suppressors including *Trp53*, *Fbxw7*, *Rock1* are strongly enriching in ESC (Fig. 2b), showing that our library is effective at gene targeting and revealing gene knockout phenotypes.

To identify common genetic dependencies of iN formation, we compared guide abundance in the ESC versus iN at D6 (Fig. 2c). Guides showing the strongest depletion are targeting, for instance, fatty acid metabolism and sterol biosynthesis, such as *Fasn*, *Hmgcr*, *Hmgcs1*, *Sqle*, an essential component for neuronal metabolism (Fig. 2c)^{41,42}. Furthermore, during iN differentiation, cells undergo high levels of stress due to lipid peroxidation and can commit cell death via apoptosis or ferroptosis^{46,47}. Hence, we find proapoptotic genes, *Casp3/9* and *Bax* enriching, while antiapoptotic genes such as *Bcl2l1* and *Sod1* are depleting from the population (Fig. 2c; Supplementary Fig. 9b). In addition, knockout of tumor suppressors, e.g., *Trp53*, *Nf1*, *Nf2*, allows for higher iN conversion. Thus, this screen yields genetic dependencies in ESC to iN conversion at high resolution.

To uncover differential genetic dependencies between iN and alternative states, relative sgRNA abundance was correlated with a particular focus on genes depleted in iN and enriched in the alternative states. We focused on differential dependencies between the Ascl1-induced iN and iT (Fig. 2d). We picked genes for validation based on the following criteria: (1) genes showing little effects in ESC ($-2 < \text{LFC} < 2$); (2) genes showing enrichment in iT ($\text{LFC} > 1.5$); (3) genes depleted in iN ($\text{LFC} < -0.5$). We noticed that genes important in the regulation of pluripotency network and differentiation of ESC: *Tcf7l1*, *Ptpn2*, *Apc*, *Strap*, *Cnot8*^{48–54}, as well as cell cycle genes *Ccnk* and *Cdk13*^{55,56} are required for Ascl1-induced iN conversion while inhibiting iT formation. In contrast, knockout of these hits had little to no influence on Ngn2-driven conversion to neurons (Fig. 2d, e).

To validate the findings, we performed a competition assay. To implement an internal control, we introduced a constitutive tagBFP vector in our cell line and derived a clone with a stable tagBFP expression. The cells were then infected with the sgRNA that showed the strongest depletion in the screen. Separately, we generated an isogenic control population, by targeting tagBFP with a control guide against tagBFP and sorting for tagBFP^{neg} cells. Subsequently, knockout and control cells were mixed in a 1:1 ratio and maintained for an additional passage to adapt them to the same conditions, before plating cells for induction (Fig. 2f). After 6 days of induction, we assessed iN Mapt-Venus-positive population, as well as Venus-negative population, corresponding to the formation of iT/iNSC populations (Fig. 2f, g). In addition, we assessed the fitness of the knockouts in the ESC cells while growing ESC for additional 6 days (Fig. 2f). As anticipated, *Sqle* was essential in iN, iT or iNSC populations, while not in ESC cells, mirroring the screen results (Fig. 2c–e, g). Similarly, knockout of pluripotency-related genes *Apc*, *Tcf7l1* and *Ptpn2* abolished the



formation of iNs upon induction with Ascl1, while allowing the formation of iT cells (Fig. 2g). We further confirmed the phenotype via immunostaining at day 6 post-induction (Fig. 2h, i). Knockout of the hits resulted in failure to generate TUBB3 positive neurons by Ascl1 while still generating CDX2+ and KRT8+ cells. Interestingly, some cells expressing neuron-specific TUBB3 lack neuronal morphology, indicating activation of neuronal genes but failure to establish a final iN

state (Supplementary Fig. 9c). Likewise, targeting of *Ccnk* or *Cdk13* strongly reduced the number of iNs upon Ascl1 induction. In contrast to Ascl1, Ngn2 iN conversion is not impaired upon loss of *Tcf711*, *Ptpn2*, and *Cdk13* and Ngn2 can still generate both neurons and neural stem cells, marked by SOX2 and PAX6 (Fig. 2g–i). However, *Apc* and *Ccnk* knockouts did affect the formation of iN and iNSC induced by Ngn2. Off note, we additionally validated multiple other genes showing

Fig. 2 | CRISPR-Cas9 forward genetic screen to identify genetic dependencies of forward differentiation by *Ascl1* or *Ngn2*. **a** CRISPR-Cas9 screen experimental outline. **b** Comparative analysis of the gene knockout effects between *Ascl1* and *Ngn2* transgenes carrying ESC. Difference in guide abundance was calculated between uninduced ESC at Day 13 post library infection (a) versus library plasmid pool. Dots represent genes; axis shows depletion in LFC in each cell line. Red represents core essential genes as defined by Hart et al.⁴⁵, blue—core pluripotency genes, yellow—tumor suppressors. **c** Comparative analysis of gene knockout effects of *Ascl1* or *Ngn2*-induced iN versus ESC. Red dots represent apoptosis related genes, yellow—tumor suppressor genes, blue—cholesterol biosynthesis genes. **d** Comparative analysis of gene knockout effects of *Ascl1*-induced iN or iT versus ESC. Red dots represent genes chosen for validation. *Sqle* is a positive control for a

strong depletion. **e** Comparative analysis of gene knockout effects of *Ngn2*-induced iN or iNSC versus ESC. Red dots represent genes chosen for validation in (d). *Sqle* is a positive control for a strong depletion. **f** Experimental outline of hits validation from (d). **g** FACS-based validation of the hits. Bar represents the normalized ratio to the initial mixture ratio at day 0. $N = 3$ independent biological replicates. Bar plot shows mean \pm SD. p -values, indicated above, were determined by one-way ANOVA followed by Dunnett's multiple comparison test (two-sided) using Ctrl ratio as a control. "n.s." not significant, "*" $p < 0.05$, "**" $p < 0.01$, "****" $p < 0.001$. **h, i** Immunostaining of the knockout cells for neuronal marker *Tubb3* and alternative lineage markers *KRT8/CDX2* for *Ascl1*-induced iT (h), and *SOX2/PAX6* for *Ngn2*-induced iNSC (i). Source data are provided as a Source Data file.

differential dependencies between *Ascl1* and *Ngn2* induction (Supplementary Fig. 9d–h). Taken together, our parallel CRISPR/Cas9 loss-of-function screens unveiled multiple common and differential dependencies between *Ascl1*- and *Ngn2*-induced directed differentiation to iNs.

Rapid downregulation of pluripotency network upon *Ascl1* induction

As the screen identified genes involved in maintaining the pluripotency network as essential for the *Ascl1*-induced iN formation, we investigated how *Ascl1* and *Ngn2* disassemble the pluripotency network in more depth. For this, we used ingenuity pathway analysis using all differential expressed genes one day post *Ascl1*- or *Ngn2*-induction (Supplementary Fig. 10a–d, Fig. 1i). As before, ingenuity canonical pathway enrichment analysis showed that both *Ascl1* and *Ngn2* induce pathways related to cholesterol biosynthesis (Supplementary Fig. 10b, d). Interestingly, the *Ascl1* transcriptional response is centered around the downregulation of the ESC pluripotency network and self-renewal (Supplementary Fig. 10a, b).

We then divided DEGs into *Ascl1* or *Ngn2* specific, or common and performed KEGG pathway enrichment analysis (Fig. 3a, b; Supplementary Fig. 10e). Interestingly, *Ascl1* upregulates genes involved in cellular senescence and cell cycle exit, such as *Cdkn1a*, *Cebpa*, *Cebpb* (Supplementary Fig. 8d, g)^{57,58}, as well as downregulates more genes involved in pluripotency, e.g., *Pou5f1* (encoding for protein OCT4), *Klf2*, *Sox2*, *Lef1*, *Lefty2*, compared to *Ngn2* (Fig. 3b, Fig. 1i, Supplementary Fig. 10e). Thus, we next looked at the dynamics of the pluripotency network (PPN) shutdown upon *Ascl1* and *Ngn2* induction. For this, we focused on the three core pluripotency genes: *Pou5f1* (Oct4), *Sox2*, *Nanog* (Fig. 3c, Fig. 1i). *Nanog* is downregulated at similar kinetics between *Ascl1* and *Ngn2* (Fig. 3c, Fig. 1i, Supplementary Fig. 11a, b). In contrast, *Sox2* expression is retained after *Ngn2* induction as an NSC gene regulatory network is established, while *Ascl1*-induced cells lose expression of *Sox2* (Fig. 3c, Fig. 1i, Supplementary Fig. 11a, b). Similarly, *Ascl1* induction leads to a rapid loss of Oct4 expression, while *Ngn2* induction leads to gradual downregulation of Oct4 (Fig. 3c–e, Fig. 1i). Furthermore, loss of Oct4 corresponds with the upregulation of trophoblast marker *KRT8* (Fig. 3f).

To test the functional relevance of the loss of Oct4, we constitutively overexpressed Oct4 and generated multiple clonal mESC cell lines (Fig. 3g, h). While overexpression of Oct4 together with *Ngn2* leads to a reduction of the iN population, co-expression of Oct4 and *Ascl1* increases the efficiency of iN formation (Fig. 3g, h). In turn, iT formation is hampered in the presence of Oct4 (Fig. 3h). During development, Oct4 inhibits differentiation of the trophoblast lineage, and rapid loss of Oct4 is associated with the upregulation of the trophoblast markers^{59,60}. Thus, rapid loss of Oct4 generates permissive conditions for iT lineage formation, that compete with the formation of iN.

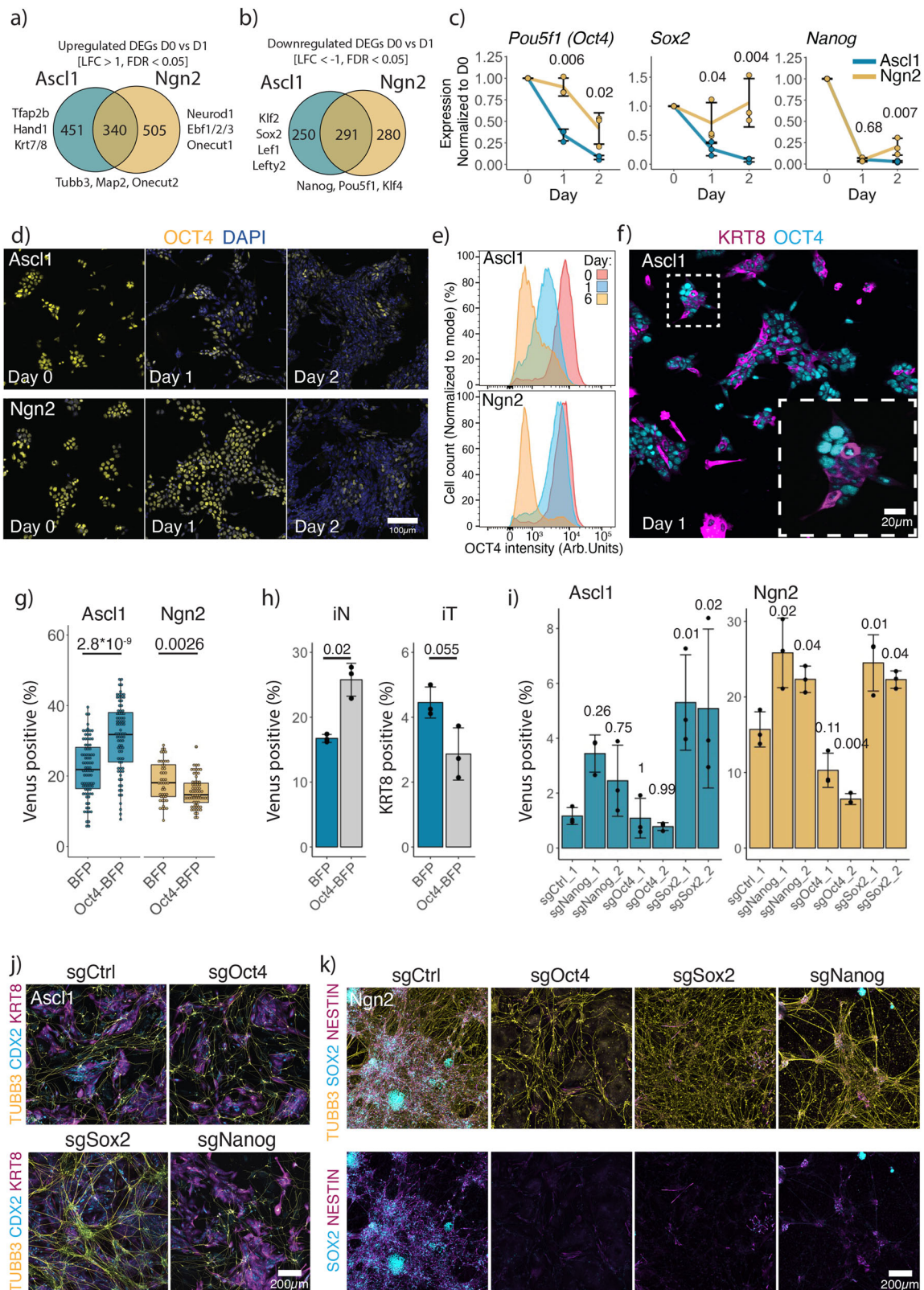
Given the kinetic differences in the downregulation of PPN after *Ascl1* or *Ngn2* induction, we tested if enforced disruption of the PPN together with differentiation would affect the ESC to iN conversion. As

Pou5f1 (Oct4), *Sox2* and *Nanog* are essential for ESC (Fig. 2b), we infected cells with the guides targeting *Pou5f1* (Oct4), *Sox2* and *Nanog* 2 days before the induction of *Ascl1* or *Ngn2* (Fig. 3i–k). Interestingly, *Ascl1* induction leads to the formation of both iN and iT in the knockout of all pluripotency factors (Fig. 3j). We see little to no effect after targeting Oct4, as Oct4 is rapidly lost upon *Ascl1* induction (Fig. 3i). However, knockout of *Nanog* or *Sox2* favors iN formation, suggesting that additional disruption of the PPN supports installment of the iN state (Fig. 3i, j). In turn, knockout of *Sox2* abolished the formation of iNSC by *Ngn2*, showing that *Sox2* is repurposed from the PPN to the NSC gene regulatory network (Fig. 3i, k). Similarly, disruption of either *Nanog* or *Pou5f1* (Oct4) also resulted in loss of iNSC (Fig. 3k). Instead, we observed formation of primitive endoderm and trophoblast upon loss of *Nanog* or *Pou5f1* (Oct4), respectively (Fig. 3k, Supplementary Fig. 11c, d), in alignment with the outcome of the loss of these factors during the development^{59–61}.

This data, together with differential dependencies identified in the CRISPR screen, shows that *Ascl1* and *Ngn2* induction leads to pronounced functional differences in exiting the pluripotency state of ESC. *Ascl1* induction leads to an efficient shutting down of PPN and later induction of iN or iT gene network, while *Ngn2* does not fully downregulate the PPN and instead overlays both networks, repurposing genes for the induction of NSCs.

Tcf7l1 is required for cell cycle exit to generate *Ascl1* iNs

We next focused on *Ascl1*-induced PPN shutdown. In *Ascl1*-driven MEF to iN transdifferentiation, *Myt1l* facilitates iN formation by repressing initial fibroblast GRN as well as alternative myoblast lineage^{16,62}. Given the fast downregulation of PPN, we tested if *Myt1l* is similarly required for ESC to iN conversion. However, our screen did not reveal that *Myt1l*, or its paralogs *Myt1* and *Stt18*, are required for ESC to iN conversion (Supplementary Fig. 12a) as well as validation experiments using additional sgRNAs (Supplementary Fig. 12b). In the CRISPR screen we identified *Tcf7l1* (T cell factor/lymphoid enhancer factor, also known as *Tcf3*), a repressor of PPN, as essential for iN formation by *Ascl1*. We confirmed the *Tcf7l1* knockout phenotype in a separate E14 background and ruled out that the loss of *Tcf7l1* affected the expression of the *Ascl1* transgene (Supplementary Fig. 12c–e). *Tcf7l1* is poised on the multiple promoters of PPN-related genes and rapidly represses their expression upon ESC differentiation^{48,63,64}, and the absence of *Tcf7l1* stabilizes the ESC state⁶⁴. Thus, we wanted to test if *Tcf7l1* is required before or after the onset of cell type conversion, as well as exclude secondary effects due to the stabilization of the PPN before the conversion. For this, we N-terminally tagged *Tcf7l1* with an Auxin inducible degron, infected cells with lentiviral vector carrying osTIR1 (F-box E3-ubiquitin ligase, derived from *Oryza sativa*) and generated single cell-derived clones (Supplementary Fig. 12f)⁶⁵. We then depleted *Tcf7l1* before or at the onset of conversion by the addition of Auxin (Supplementary Fig. 12g). While *Tcf7l1* depletion before induction had only a mild effect on the formation of iN, degrading *Tcf7l1* on the onset of *Ascl1* induction severely reduced the number of neurons produced by



Ascl1 (Supplementary Fig. 12g). This indicates that *Tcf7l1* acts after the induction rather than stabilizing the PPN.

To understand the role of *Tcf7l1* in the Ascl1-induced ESC to iN-directed differentiation, we generated single cell-derived clones with a homozygous *Tcf7l1* knockout and performed bulk RNAseq at day 1 post-induction (Supplementary Fig. 13a). As *Tcf7l1* acts as a pluripotency network repressor during ESC differentiation, we first looked at the

pluripotency shutdown in the *Tcf7l1* knockout cells. Surprisingly, the PPN was still downregulated after Ascl1 induction in the absence of *Tcf7l1* (Fig. 4a; Supplementary Fig. 13a). However, we observed a group of genes that failed to be expressed in $\Delta Tcf7l1$ clones (Supplementary Fig. 13a). Interestingly, *Cdkn1c* is highly upregulated after Ascl1 induction in comparison to $\Delta Tcf7l1$ (Supplementary Fig. 13a), and its expression is specific for Ascl1 induction and peaks at day 3 of ESC to iN

Fig. 3 | Dynamics of pluripotency network shutdown. **a, b** Number of *Ascl1*, *Ngn2* specific or common upregulated (**a**) and downregulated (**b**) genes from Fig. 1i. **c** qPCR data of the expression of the core pluripotency genes (normalized to the expression of Actin and day 0). Lines are drawn through the mean of $n = 3$ biologically independent samples; error bars indicate \pm SD. Above, p -values of the two-sided Welch two-sample t -test comparing PPN genes expressed between *Ascl1* and *Ngn2* at the given time point. **d** Representative immunostainings for the OCT4 dynamics after *Ascl1* or *Ngn2* induction. **e** Quantification of OCT4 expression using intracellular immunostaining followed by FACS. **f** Representative immunostaining for the pluripotency marker OCT4 and trophoblast marker KRT8 at day 1 after *Ascl1* or *Ngn2* induction. **g** Efficiency of iN formation in the presence of OCT4 over-expression. Each dot represents an individual ESC clone containing an over-expression construct. Efficiency is measured by the percentage of Mapt-Venus population. Boxplots indicate 25th and 75th percentiles as bounds of the box with

the median center line; whiskers indicate minima/maxima of a 1.5x distance of the IQR from the 25th and 75th percentiles. p -value of the two-sided Welch two-sample t -test indicated above. **h** Efficiency of iN formation, measured by the percentage of Mapt-Venus expressing cells, and iT formation, percentage of cells immunostained for KRT8 of polyclonal population overexpressing Oct4-BFP. Bar plot shows mean of $n = 3$ independent biological replicates with \pm SD; the p -values were calculated using the two-sided Welch two-sample t -test. **i** Efficiency of iN formation upon acute knockout of core pluripotency. Efficiency is measured by the percentage of Mapt-Venus population. The bar plot shows mean of $n = 3$ biologically independent samples with \pm SD. p -values, indicated above, were calculated using one-way ANOVA followed by Dunnett's multiple comparison test (two-sided) using sgCtrl as a control. **j** Representative immunostainings of (i) for iN and iT induced by *Ascl1*. **k** Representative immunostainings of (i) for iN and iNSC induced by *Ngn2*. Source data are provided as a Source Data file.

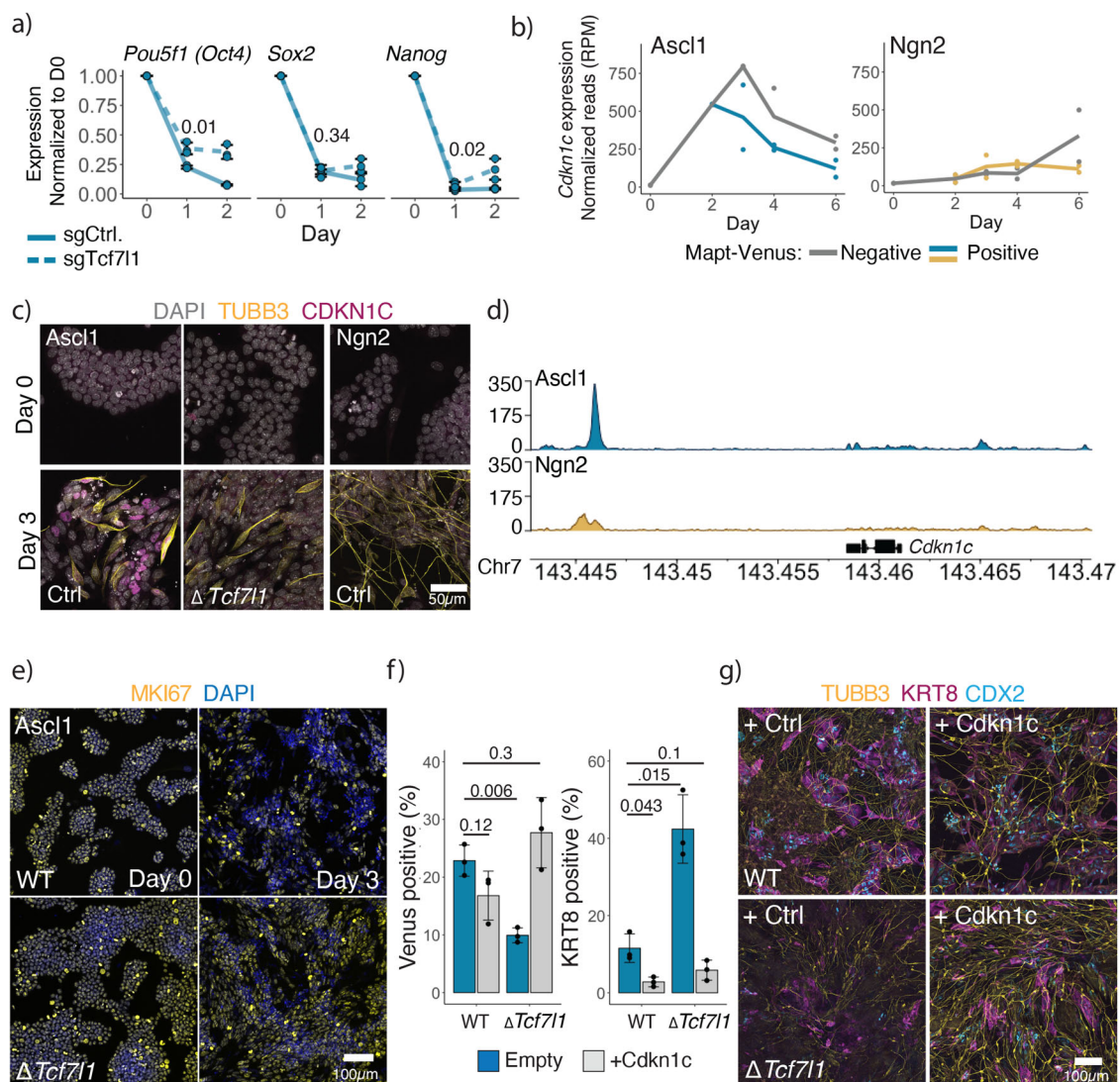


Fig. 4 | Overexpression of *Cdkn1c* rescues *Tcf7l1* knockout phenotype. **a** qPCR of core pluripotency gene expression after induction in WT and *Tcf7l1* KO cells. Expression normalized to Actin and day 0. Lines are drawn through the mean of $n = 3$ biologically independent samples; error bars indicate \pm SD. p -values of the two-sided Welch two-sample t -test comparing sgTcf7l1 vs sgControl at day 1 indicated above. **b** *Cdkn1c* expression during ESC to iN conversion (Fig. 1a). **c** Immunostainings of CDKN1C on day 0 and day 3 of the ESC to iN conversion by *Ascl1* WT or *Tcf7l1* KO or *Ngn2* expressing cells. **d** Binding of the Flag-*Ascl1* or Flag-*Ngn2* in the *Cdkn1c* locus at day 1 post-induction. Data showing combined reads of four replicates. **e** Immunostainings of proliferation marker MKI67 after induction of *Ascl1* in

WT or *Tcf7l1* KO ESC cells. **f** FACS data of *Cdkn1c* overexpression with *Ascl1* in WT or *Tcf7l1* KO ESCs. The efficiency of iN formation is measured by the percentage of Mapt-Venus population, efficiency of iT formation is measured by the percentage of cells immunostained for KRT8. The bar plot shows mean of $n = 3$ independent biological replicates with \pm SD. p -value of the two-sided Welch two-sample t -test indicated above. **g** Representative images of immunostained cells for neuronal TUBB3 and trophoblast CDX2/KRT8 markers at day 6 post-induction of WT or *Tcf7l1* KO ESCs with *Ascl1* and *Cdkn1c*. Source data are provided as a Source Data file.

conversion (Fig. 4b, c; Supplementary Fig. 13b). In addition, Ascl1 shows strong binding near *Cdkn1c* locus in comparison to Ngn2 (Fig. 4d).

Ascl1-directed differentiation is cell cycle-dependent

Cdkn1c is a cyclin-dependent kinase inhibitor of the cip/kip family regulating cell cycle arrest in G1⁶⁶. *Cdkn1c* is essential for embryonic development, and mice lacking *Cdkn1c* die perinatally with multiple developmental defects. Furthermore, *Cdkn1c* is important for the development of early placenta to initiate the endoreplication of trophoblasts⁶⁶. Recently, *Cdkn1c* was also implicated in the suppression of pluripotency in mouse ESC⁶⁷. We furthermore see that Ascl1-induced GRN central nodes contain multiple genes involved in cell cycle regulation, e.g., *Cdkn1a*, *Cdkn1b*, *Cebpa*, *Cebpb* (Supplementary Fig. 8d, g). Thus, we hypothesized that in Δ *Tcf7l1* cells, Ascl1 is unable to arrest the cell cycle. Indeed, we observe prolonged expression of MKI67 as well as a higher percentage of dividing cells after induction of Ascl1 in the Δ *Tcf7l1* cells (Fig. 4e, Supplementary Fig. 13c). To test if the expression of *Cdkn1c* is sufficient to induce iN formation in the absence of *Tcf7l1*, we coexpressed *Cdkn1c* together with Ascl1. Indeed, we see a partial rescue of iN formation as well as a decrease in iT generation (Fig. 4f, g). Furthermore, we see that expression of *Cdkn1c* generates a more mature neuronal and trophoblast phenotype also in WT populations by Day 6 (Fig. 4g). Of note, *Cdkn1c* is not essential for the formation of Ascl1-induced iNs, suggesting that a group of cell cycle regulators, rather than *Cdkn1c* alone, is responsible for the cell cycle arrest (Supplementary Fig. 13d).

Taken together, our data show that in Ascl1-induced ESC to iN conversion, cell cycle arrest is a roadblock after exiting the pluripotency state and that *Cdkn1c* is sufficient to overcome this roadblock. In contrast, this dependency is not observed for Ngn2-dependent iN formation, where the cell cycle is maintained and some ESCs transit to NSCs.

Discussion

Overexpressing proneural bHLH transcription factors Ascl1 or Ngn2 in mouse ESC show several differences in the conversion toward iN: (1) formation of different alternative lineages; (2) early transcriptional changes in downregulation of pluripotency network and upregulation of new transcripts; (3) different genetic dependencies. In addition to iN, Ascl1 induces trophoblast-like cells marked by *Krt8* and *Cdx2*, while Ngn2 invokes an NSC-like state³⁸. The induction of alternative states results from the binding and upregulation of alternative lineage specifying factors, e.g., *Hand1*, *Cdx2* in Ascl1 case and *Pax3* in Ngn2. To induce trophoblast lineage, Ascl1 in mESC acts similarly to Ascl2, a key trophoblast lineage driving the bHLH transcription factor. Interestingly, during MEF to iN transdifferentiation, Ascl1 also binds trophoblast lineage drivers in MEF, although without inducing them (Supplementary Fig. 7a, b). Instead, additionally to iN, Ascl1 expressed in MEF induces myocyte-like cells^{16,19}. In turn, muscle lineage genes and other targets are bound in both ESC and MEF^{16,19} (Supplementary Fig. 7c, d). Thus, besides the neuronal lineage, only those Ascl1-bound genes are induced, which are developmentally close to the initial cell lineage in which Ascl1 is expressed. Differences in epigenetic landscape, histone modifications around binding targets as well as interaction partners or cofactors present in the initial cell types could specify binding and induction of target genes molding the mechanism^{6–9,12,14}. Thus, the iN conversion paradigm from different cell types using the same transcription factor provides a powerful experimental platform to study how transcription factors binding and induction of lineages can be affected by cellular context.

An important aspect of lineage conversion is the efficient inhibition of the initial cell type. Overcoming the initial state is a well-described bottleneck in reprogramming to iPSC cells^{58,69}, and utilizing efficient initial lineage repression would require fewer cues to install a new cell identity. For example, miRNA-induced neuronal

reprogramming of fibroblasts primarily acts via repression of the REST complex and non-neuronal factors, highlighting the importance of repression of the initial cell state⁷⁰. Even though Ascl1 acts primarily as a transcriptional activator⁶, we show that Ascl1 rapidly downregulates the PPN. *Pou5f1* (*Oct4*) and *Nanog* are lost within 24 h upon Ascl1 expression, and *Sox2* is largely downregulated after 48 h. Similarly, MEF gene regulatory network is rapidly disassembled upon Ascl1 expression⁷¹. However, the Ascl1-induced pluripotency repression mechanism is yet to be addressed.

We conducted comparative forward genetic screens to systematically elucidate the genetic dependencies of both Ascl1 and Ngn2-induced transitions. Interestingly, Ascl1 transition was more dependent on the factors modulating the PPN and cell cycle. We selected *Tcf7l1*, a well-described PPN repressor, as a representative of this gene group. Surprisingly, the PPN was still downregulated even after *Tcf7l1* knockout. However, we noticed that Ascl1 fails to induce *Cdkn1c* in the absence of *Tcf7l1*. This suggests that exit from the cell cycle might be a prerequisite for Ascl1-driven neuronal conversion. Indeed, co-expression of *Cdkn1c* with Ascl1 triggered cell cycle exit and rescued the loss of *Tcf7l1*. Taken together, the ability of Ascl1 to rapidly downregulate the initial cell state and effectively induce cell cycle arrest can be an inherent part of its strong transdifferentiation potential across large developmental distances^{27,72}. In such a case, efficient downregulation of the initial network would also allow easier installment of the new cellular state even from the weaker GRN induced by Ascl1. However, multiple signals induced by Ascl1 in the absence of initial state GRN would also allow permissive conditions for installing alternative cell fates, e.g., iT in ESC and myocyte in MEF.

In contrast, Ngn2 induces a stronger and more interconnected and self-sustaining network than Ascl1 in ESC. Indeed, Ngn2 gives rise to iN cells faster and more efficiently (Supplementary Fig. 1a). Similarly, Ngn2 binds to and induces more targets than Ascl1 also in human fibroblasts, including proneural genes like *NEUROD1* and *NEUROD4*^{73,74}. Yet, only Ascl1 alone is sufficient to convert MEFs to functional neurons, while Ngn2 requires the addition of small molecules to facilitate genome accessibility^{74,75} or co-expression with additional transcriptional activators such as *Brn3a*^{76,77}. This discrepancy could, at least in part, be explained by weaker repression of the initial state by Ngn2. For example, co-expression of transcriptional inhibitors, such as *Myt1l*, together with Ngn2 leads to successful MEF to iN conversion^{62,76}. However, despite strong proneural GRN upregulation, Ngn2 induction leads to slower and incomplete repression of PPN after induction in ESC. This is indicative by the formation of trophoblast or primitive endoderm cells forming after and acute knockout of *Nanog* or *Oct4*, respectively, driven by the residual PPN^{59–61}. Furthermore, Ngn2 retains *Sox2* expression as part of the NSC GRN, which acts as a proliferative intermediate. Thus, in ESCs, Ngn2 appears to overlay the PPN with neuron-specific genes and thereby generate a feed-forward loop to drive neuron formation with the appearance of NSC.

These observations indicate that Ascl1 and Ngn2 utilize different mechanisms to transition cells between identical states, namely from mESC to the same iN subtype. Specifically, Ascl1 dismantles one fate followed by the installment of another, while Ngn2 overlays the cell identities toward a new cell fate in a development-like process.

Methods

The experiments in this study are in compliance with relevant guidelines and ethical regulations.

Cell culture

Mouse ESCs (mESCs) were maintained in ESCM medium: DMEM (Sigma, D1152) supplemented with 15% Fetal bovine serum (FBS, Gibco, 10270106), 100 U/ml Penicillin, 100 µg/ml Streptomycin (Sigma, P0781), 1x Non-essential amino acids (Sigma, M7145), 4 mM L-Glutamine (Sigma, G7513), 1 mM Na-Pyruvate (Sigma, S8636), 0.1 mM

β -mercaptoethanol (Merck, 805740), 50 μ g/ml ascorbic acid, 1000 U/ml LIF (ESGRO Millipore). Cells were trypsinized and replated every second day on gelatin-coated plates with the irradiated DR4 mouse embryonic fibroblasts (MEF) feeders, isolated from the E13.5 stage embryo of the DR4 mouse strain (RRID:MSR_JAX:003208), plated a day before.

For iN induction, mESC were trypsinized, and 10^8 cells per well were plated on Matrigel (1 h 37 °C, 300 μ L of 1000x diluted Matrigel (Szabo Scandic, BDL356231)) in a 24 well in the evening. The next day cells were washed twice with PBS and induced with N2B27 medium: DMEM/F12 (Gibco, 10565018), Neurobasal (Gibco, 21103049), N2 supplement (Gibco, 17502048), B27 supplement (Gibco, 17504044), 100 U/ml of Penicillin, 100 μ g/ml Streptomycin (Sigma, P0781), 1x Non-essential amino acids (Sigma, M7145), 4 mM of L-Glutamine (Sigma, G7513), 1 mM of Na-Pyruvate (Sigma, S8636), 20 μ g/ml Insulin (Roche, 15898200), 1 μ g/ml doxycycline (dox). Time of induction was considered as day 0. From Day 2 onward, half of the medium was exchanged daily. For the induction of the iNSC state, cells were grown in the presence of 20 ng/ml FGF2 (PeproTech, 450-33) and 20 ng/ml EGF (PeproTech, 315-09). To enrich for non-dividing cells, 4 μ M cytosine β -D-arabino-furanoside (AraC, Sigma-Aldrich) was added from day 4 onward. Cells were dissociated with trypsin and quantified using FACS BD LSR Fortessa (BD Biosciences). Subsequent gating of the data was done using FlowJo (BD Biosciences, v10.8.1).

Cell lines

Doxycycline-inducible TetO-Ascl1 and TetO-Ngn2 mouse ESC lines were established as described previously⁷. Cells were then infected with a lentiviral construct containing constitutive Cas9, and single cell-derived clones were tested for stable Cas9 expression and robust ESC to iN conversion. Plasmid containing V5-P2A-Venus-T2A-PuroTK-LoxP-Efla-Neo-LoxP tag flanked with 750 bp homology arms adjacent to *Mapt* terminus was co-electroporated with a CRISPR-Cas9 sgRNA targeting *Mapt* gene C-terminus (Supplementary Table 1) using Mouse Embryonic Stem Cell Nucleofector™ kit (Lonza) and selected with 0.5 mg/ml G418 (Gibco). Neomycin resistance was excised via transfection of the plasmid containing Cre and individual clones were derived, genotyped, and tested for the reporter activity via FACS and immunostaining.

Individual clones with *Tcf7l1* knockouts were derived by infecting cells with the lentiviral vector containing sgRNA targeting *Tcf7l1* (Supplementary Table 1), mutagenizing for 7 days and subsequent picking of the single cell-derived clones. The correct genotype was confirmed by Sanger sequencing of the endogenous *Tcf7l1* locus and western blot.

N-terminus *Tcf7l1* tagging with AID degron was done by co-electroporating plasmid containing mCherry-V5-AID flanked by 1 kbp homology arms and a plasmid with sgRNA targeting *Tcf7l1* start codon. Successful homozygous integration in single cell-derived clones was confirmed via genotyping and western blot. Cells were infected with lentiviral vector delivering pSFFV-ostTIR-T2A-eBFP2 and single cell-derived clones were tested for degradation of *Tcf7l1*, retained BFP expression during differentiation and showed no hypomorphic effects on iN conversion without induction of degradation.

An alternative cell line for validations of the formation of alternative lineages and ChIP-seq experiments was derived by electroporating E14 mESC (RRID:CVCL_C320) with piggyBac vector containing CAG-rtTA-IRES-Hygro (Addgene plasmid number #102423) and a plasmid with piggyBac transposase. Cells were then infected with a lentiviral construct containing Tet-O-FLAG-Ascl1-T2A-Puro or Tet-O-FLAG-Ngn2-T2A-Puro (modified from Addgene plasmid #52047) and single cell-derived clones were subsequently tested for the resistance to puro after dox addition.

To confirm the *Tcf7l1* knockout phenotype, cells were derived in triplicates in the same way described in the ChIP experiment, but

without clonal expansion. Cells were then infected with an U6-sgTcf7l1-PGK-Cas9-P2A-Blast lentiviral vector, selected with 10 μ g/ml blasticidin (Invivogen) for 4 days, and mutagenized for a week before assessing the phenotype.

For Cdkn1c co-expression with Ascl1, cells were infected with Tet-O-Cdkn1c-T2A-Puro (modified from Addgene plasmid #52047) vector. After 3 days, cells were induced as described above. From day 1, Cdkn1c expression was selected with 1 μ g/ml Puromycin (Invivogen).

For PPN perturbation experiments, sgRNAs against *Nanog*, *Pou5f1*, *Sox2* were cloned into spCas9-P2A-Puro vector. One day post-infection, cells were selected with 1 μ g/ml Puromycin (Invivogen) for a day. A kill control without Puromycin resistance cassette was used to ensure complete selection. Cells were then split and induced with Dox, as described above.

SgRNA cloning and virus preparation

Individual sgRNAs (Supplementary Table 1) were cloned into the lentiviral plasmid containing spCas9-P2A-Blast using the single guide RNA Gecko cloning protocol (<https://www.addgene.org/crispr/zhang>). Lentiviral vectors were transfected using Polyethylenimine (PEI) into Lenti-X (Clontech, 632180) for virus production according to the supplier's recommendations. Virus containing supernatant was filtered through a 0.45 μ m PES filter (VWR). For infection, 10^8 mESC were plated per gelatin-coated well in a 24-well plate. After recovery for at least 4 h, cells were infected with virus diluted 2x in fresh ESCM. The next day medium was exchanged and irradiated DR4 MEF feeders were plated on top of ESC. Successful integrations were selected with 10 μ g/ml blasticidin for 4 days.

Immunofluorescence

Cells were grown and differentiated on the Matrigel-coated glass coverslips. Cultured cells were then gently washed with PBS, fixed for 15 min at room temperature with 4% paraformaldehyde (PFA) in PBS. Cells were washed twice with PBS and subsequently permeabilized and blocked with blocking solution (5% FBS, 0.1% Triton™ X-100 in PBS) for 1 h at room temperature. Then coverslips were incubated with primary antibody overnight at 4 °C. Used primary antibodies were mouse anti-TUBB3 (Sigma, T8660, 1:500), rabbit anti-TUBB3 (Biolegend/Covance, PRB-435P, 1:500), rabbit anti-MAP2 (Abcam, ab32454, 1:500), rat anti-SOX2 (Invitrogen (eBioscience), 14-9811-80, 1:500), rabbit anti-OCT4 (Abcam, ab19857, 1:500), rabbit anti-NANOG (Abcam, ab80892, 1:500), rabbit anti-PAX6 (Covance, PRB-278P, 1:200), rat anti-KRT8/TROMA-1 (DSHB, AB 531826, 1:200), rabbit anti-CDX2 (Abcam, ab76541, 1:400), mouse anti-Nestin (Merk, MAB353, 1:200), rat anti-GATA4 (Invitrogen, 14998082, 1:500), rabbit anti-CDKN1C (Abcam, ab75974, 1:250), rat anti-Mki67 (Invitrogen (eBioscience), 14-5698-82, 1:200), mouse anti-ASCL1 (Invitrogen (eBioscience), 14-5794-82, 1:200), rabbit anti-TPBPA (Abcam, ab104401, 1:200). Coverslips were washed three times with PBS 5 min at room temperature while gently rocking, and then incubated with secondary antibody in blocking solution for 1 h at room temperature. DAPI (0.5 μ g/ μ l) was added together with a secondary antibody. Secondary antibodies used: goat anti-Mouse-488 (Invitrogen, A11029, 1:1000), goat anti-Rabbit-488 (Invitrogen, A11034, 1:1000), goat anti-Rat-488 (Invitrogen, A11006, 1:1000), goat anti-Mouse-568 (Invitrogen, A11031, 1:1000), goat anti-Rabbit-568 (Invitrogen, A11036, 1:1000), goat anti-Mouse-647 (Invitrogen, A21247, 1:1000), goat anti-Rabbit-647 (Invitrogen, A21236, 1:1000), goat anti-Rat-647 (Invitrogen, A21245, 1:1000). Coverslips were then washed as before and mounted on glass using Prolong™ Glass Antifade Mountant (Invitrogen, P36984).

For flow cytometry experiments with intracellular immunostaining of cells (FACS-IF), cells were grown as described above, dissociated with trypsin, washed with PBS and fixed for 15 min at room temperature with 4% PFA in PBS. Cells were then washed with PBS and 50–100 μ l of cell suspension were pelleted at 400 \times g for 5 min,

permeabilized and blocked with 100 μ l blocking solution for 1 h at room temperature. Cells were then centrifuged at 400 \times g for 5 min and washed twice with 200 μ l PBS. Cells were incubated with primary antibody (same as for microscopy samples) in the blocking solution for 1 h at room temperature, washed twice with 200 μ l PBS with 400 \times g 5 min centrifugation in between, and incubated with secondary antibody (same as for microscopy samples) and DAPI (0.5 μ g/ μ l) in the blocking solution for 1 h at room temperature. Cells were washed twice with 200 μ l PBS and resuspended in 100 μ l PBS and quantified using FACS BD LSR Fortessa (BD Biosciences).

RT-qPCR

Total RNA was extracted using the Qiagen RNeasy mini kit. Then, 1–2 μ g of total RNA was reverse transcribed using the SuperScript[™] III Reverse Transcriptase (Invitrogen). RT-qPCR was performed using GoTaq[®] qPCR MasterMix (Promega). RT-qPCR primer sequences used in this study can be found in Supplementary Table 3. Relative RNA levels were calculated from C_t values by the standard $\Delta\Delta C_t$ method and normalized to *Actin* mRNA levels.

Screen

Retroviral CRISPR-UMI sgRNA library was produced by transfection of the PlatinumE cells (Cell Biolabs) as described before⁴⁴. In the morning, 3×10^8 ESC were plated on the gelatin-coated plates (10^7 cells per plate) without feeders and infected with a 10% infection rate 1 h later. In the evening, feeders were seeded on top of the ESC. Successfully infected cells were selected with 0.5 mg/ml G418 (Gibco, 11811-031) for 5 days changing medium daily and splitting while maintaining 500 \times library coverage at all times. Nine days post-infection, 5×10^6 cells per plate were plated on Matrigel-coated 15 cm plates in the morning and induced with N2B27+Dox medium in the evening with a total of 6×10^7 cells per condition. Half of the medium was exchanged daily. From day 4 onward, iN were purified by the addition of 4 μ M cytosine β -D-arabinofuranoside (AraC, Sigma-Aldrich) and 1 μ g/ml puromycin until day 6 post-induction. For the iNSC samples, cells were trypsinized and expanded after day 3 post-induction for additional 4 days in N2B27+Dox medium containing 20 ng/ml FGF2 (PeproTech, 450-33) and 20 ng/ml EGF (PeproTech, 315-09). iT were enriched by plating cells at day 6 in ESCM after trypsinization onto gelatin-coated 15 cm plates for 20 min and then washing off unattached cells with PBS. ESC were kept in parallel in ESCM medium and feeders as described above. At the end of differentiation, cells were trypsinized, washed with PBS, pelleted by centrifugation at 300 \times g for 5 min and frozen. Lastly, gDNA isolation, PacI digestion (NEB), size selection, PCR amplification and NGS were carried out as previously published^{44,78}.

RNAseq

Cells were collected at 0 h, 24 h and 48 h post-induction as bulk samples, and on days 3, 4, and 6, cells were sorted into Venus-positive and Venus-negative cells using FACS Aria III (BD bioscience). Cells were washed with PBS and processed using the Qiagen RNeasy mini kit. RNA was additionally treated with a TURBO DNA-free[™] kit (Invitrogen) according to the manufacturer's protocols. The integrity of RNA was measured using Fragment Analyzer[™] (Advanced Analytical). RNAseq-Libraries were prepared using QuantSeq 3' mRNA-Seq Library Prep Kit (Lexogen GmbH). LUTHOR 3'-scRNAseq (Lexogen GmbH) libraries were prepared using the manufacturer's protocol after sorting cells into 5 μ l lysis agent. Concentrations and distributions of the libraries were checked with the Fragment Analyzer[™] using HS NGS Fragment Kit (Agilent; DNF-474-0500). Libraries were then pooled and sequenced using Illumina Nextseq550 in a single read 75 cycles run.

ChIPseq

Two replicates of 25×10^6 E14 (CAG-rtTA-Hygro, LV-TetOL-Flag-Ascl1/Ngn2-T2A-Puro) cells were collected 24 h after induction, washed

with PBS and fixed with 1% freshly prepared formaldehyde (FA) solution in PBS for 7 min at room temperature. FA was then quenched with 0.125 M glycine. Nuclei were extracted by cell lysis in 50 mM HEPES-KOH pH 8.0, 140 mM NaCl, 1 mM EDTA, 10 % glycerol, 0.5% NP40, 0.25 % Triton X-100 for 10 min at 4 °C, followed by 5 min on ice in 10 mM Tris-HCl pH 8.0, 1 mM EDTA, 0.5 mM EGTA, 200 mM NaCl. Nuclei were then washed and resuspended in 10 mM Tris-HCl pH 8.0, 0.1 % SDS, 1 mM EDTA with 1 \times Complete mini protease inhibitors (Roche), and chromatin was sheared using Covaris E220 High Performance Focused Ultrasonicator (Duty factor 5.0, PIP 140.0, 200 cycles per burst at 4 °C). Fragment sizes of 250–800 bp were confirmed via agarose gel electrophoresis. 1% of fragmented chromatin was kept as an input sample. For each replicate, a duplicate of 50 μ g of chromatin was used for overnight 4 °C incubation with 5 μ g of anti-FLAG (Sigma, F1804) in IP Buffer (50 mM HEPES-KOH pH 7.5, 140 mM NaCl, 1 mM EDTA, 1% Triton X-100, 0.1% DOC, 0.1% SDS) with BSA blocked Protein G coupled Dynabeads (Thermo Fisher Scientific; Blocking was done for 3 h at 4 °C). Beads were then washed eight times with IP buffer and once with TE, 50 mM NaCl. The DNA was eluted twice with 150 μ l of 1% SDS, 0.1 M NaHCO₃ for 20 min at 65 °C. The eluate was then treated with RNase A and Proteinase K and reverse crosslinked overnight at 65 °C. DNA was purified using phenol/chloroform extraction and isopropanol precipitation. ChIP libraries were prepared using the NEBNext Ultra-II kit (New England Biolabs) following the manufacturer's protocol. The quality of the libraries was assessed with the Fragment Analyzer[™] using HS NGS Fragment Kit, and libraries were sequenced using Illumina HiSeq V4 in a single read 50 bp sequencing run.

Data analysis

RNAseq. RNA-seq reads were trimmed using BBDuk v38.06 (ref=polyA.fa.gz, truseq.fa.gz k = 13 ktrim=r useshortkmers=t mink=5 qtrim=r trimq=10 minlength=20) and reads mapping to abundant sequences included in the iGenomes Ensembl GRCm38 bundle (mouse rDNA, mouse mitochondrial chromosome, phiX174 genome, adapter) were removed using bowtie2 v2.3.4.1 alignment. The remaining reads were analyzed using genome and gene annotation for the GRCm38/mm10 assembly obtained from *Mus musculus* Ensembl release 94. Reads were aligned to the genome using star v2.6.0c, and reads in genes were counted with featureCounts (sub-read v1.6.2) using strand-specific read counting for QuantSeq experiments (-s 1). For differential expression analysis and variance stabilized transformation for PCA analysis, we used R package Deseq2⁷⁹ (v.1.32.0). Significantly differentially expressed genes (DEG) were considered those genes with FDR < 0.05 and $-1 < \text{Log}_2(\text{Fold change}) < 1$. For the KEGG pathway enrichment analysis and identification of the alternative cell lineages using the PanglaoDB database³², we used Enrichr⁸⁰. For the DEG network analysis and visualization, we used the STRING database and Cytoscape (v.3.8.0).

ChIPseq. ChIP-seq reads were trimmed using trim-galore v0.4.4 and thereafter aligned to the mm10 reference genome using bwa mem v0.7.17. Duplicated reads were removed using Picard MarkDuplicates (v2.23.4.). Complexity and overall data quality were assessed using phantompeakqualtools and deepTools plotFingerprint (v 3.5.0). To generate bigwig files from corresponding bam files, we used deepTools bamCoverage (v 3.5.0), with parameter -normalizeUsing RPKM. Peak calling from the sorted BAM files was done using MACS2 (v2.1.1). Peaks in blacklist regions were identified using bedtools intersect (v2.27.1) and mm10.blacklist.bed.gz v1. To analyze overlapping and unique peaks between Ascl1 and Ngn2, as well as plotting peak heatmaps, we used the R package Diffbind⁸¹ (v3.2.7) with minOverlap = 4 to collapse replicates after making a consensus peaksets. For determining binding motifs, we used MEME-ChIP (v5.1.1) with -meme-minw 6 -meme-maxw 15 parameters. For

plotting the binding profiles, we combined the reads from the replicates using UCSC bigWigMerge and used R package karploter (v1.18.0).

CRISPR-Cas9 screen analysis. Analysis of CRISPR-Cas9 screens was done according to previously published protocol^{44,78}. In short, reads were trimmed to 20 nt sgRNA sequence using fastx-toolkit (v0.0.14) and mapped to reference sequences using bowtie (v1.1.2). Experimental indices and mapped reads were collapsed into count tables using in-house Python scripts. Gene enrichment was determined using MAGeCK⁸² (v0.5.4). Visualization was done using the R package ggplot2 (v3.3.6).

Statistics and reproducibility. Experiments were independently performed at least three times (unless otherwise stated). Figure 3g screen validation experiment, a replicate was excluded for Setd1b due to an inefficient number of cells, thus resulting in poor sample quantification. No key conclusions were drawn based on this sample. Results are reported as mean \pm SD. For comparing between two groups, a two-tailed unpaired Student's *t*-test was performed. One-way ANOVA followed by Dunnett's multiple comparison test was applied for comparisons of multiple groups. Statistical tests were performed using R. Only representative micrographs are shown from at least two independent replicates, as similar results were obtained between replicates. In Supplementary Figs. 4, 12c–d, micrographs of all the replicates are shown.

Reporting summary

Further information on research design is available in the Nature Portfolio Reporting Summary linked to this article.

Data availability

Raw NGS data produced in this study have been deposited in Gene Expression Omnibus (GEO) database under super series accession number [GSE206872](#): ChIP-seq ([GSE206869](#)), RNA-seq ([GSE206870](#), [GSE208199](#)), CRISPR-Cas9 screen ([GSE206871](#)). Single-cell RNA-seq data for reanalysis can be obtained from [GSE125620](#)⁹. Source data are provided with this paper.

Code availability

Only standard bioinformatic code was used for the data analysis and is available on request.

References

- Balsalobre, A. & Drouin, J. Pioneer factors as master regulators of the epigenome and cell fate. *Nat. Rev. Mol. Cell Biol.* **23**, 449–464 (2022).
- Bergsland, M. et al. Sequentially acting Sox transcription factors in neural lineage development. *Genes Dev.* **25**, 2453–2464 (2011).
- Buecker, C. et al. Reorganization of enhancer patterns in transition from naive to primed pluripotency. *Cell Stem Cell* **14**, 838–853 (2014).
- Holmberg, J. & Perlmann, T. Maintaining differentiated cellular identity. *Nat. Rev. Genet.* **13**, 429–439 (2012).
- Li, M. & Belmonte, J. C. I. Ground rules of the pluripotency gene regulatory network. *Nat. Rev. Genet.* **18**, 180–191 (2017).
- Aydin, B. et al. Proneural factors *Ascl1* and *Neurog2* contribute to neuronal subtype identities by establishing distinct chromatin landscapes. *Nat. Neurosci.* **22**, 897–908 (2019).
- Wapinski, O. L. et al. Hierarchical mechanisms for direct reprogramming of fibroblasts to neurons. *Cell* **155**, 621–635 (2013).
- Ali, F. R. et al. The phosphorylation status of *Ascl1* is a key determinant of neuronal differentiation and maturation in vivo and in vitro. *Development* **141**, 2216–2224 (2014).
- Azzarelli, R. et al. *ASCL1* phosphorylation and *ID2* upregulation are roadblocks to glioblastoma stem cell differentiation. *Sci. Rep.* **12**, 2341 (2022).
- Blomfield, I. M. et al. *Id4* promotes the elimination of the pro-activation factor *Ascl1* to maintain quiescence of adult hippocampal stem cells. *eLife* **8**, e48561 (2019).
- Han, S. et al. Proneural genes define ground-state rules to regulate neurogenic patterning and cortical folding. *Neuron* **109**, 2847–2863.e11 (2021).
- Le Dréau, G. et al. E proteins sharpen neurogenesis by modulating proneural bHLH transcription factors' activity in an E-box-dependent manner. *eLife* **7**, e37267 (2018).
- Viñals, F. et al. BMP-2 decreases *Mash1* stability by increasing *Id1* expression. *EMBO J.* **23**, 3527–3537 (2004).
- Herrero-Navarro, Á. et al. Astrocytes and neurons share region-specific transcriptional signatures that confer regional identity to neuronal reprogramming. *Sci. Adv.* **7**, eabe8978 (2021).
- Urbán, N. et al. Return to quiescence of mouse neural stem cells by degradation of a proactivation protein. *Science* **353**, 292–295 (2016).
- Lee, Q. Y. et al. Pro-neuronal activity of *Myod1* due to promiscuous binding to neuronal genes. *Nat. Cell Biol.* **22**, 401–411 (2020).
- Nishiyama, A. et al. Uncovering early response of gene regulatory networks in ESCs by systematic induction of transcription factors. *Cell Stem Cell* **5**, 420–433 (2009).
- Schiebinger, G. et al. Optimal-transport analysis of single-cell gene expression identifies developmental trajectories in reprogramming. *Cell* **176**, 928–943.e22 (2019).
- Treutlein, B. et al. Dissecting direct reprogramming from fibroblast to neuron using single-cell RNA-seq. *Nature* **534**, 391–395 (2016).
- Briggs, J. A. et al. Mouse embryonic stem cells can differentiate via multiple paths to the same state. *eLife* **6**, e26945 (2017).
- Lin, H.-C. et al. *NGN2* induces diverse neuron types from human pluripotency. *Stem Cell Rep.* **16**, 2118–2127 (2021).
- Mertens, J., Marchetto, M. C., Bardy, C. & Gage, F. H. Evaluating cell reprogramming, differentiation and conversion technologies in neuroscience. *Nat. Rev. Neurosci.* **17**, 424–437 (2016).
- Wang, H., Yang, Y., Liu, J. & Qian, L. Direct cell reprogramming: approaches, mechanisms and progress. *Nat. Rev. Mol. Cell Biol.* **22**, 410–424 (2021).
- Bocchi, R., Masserdotti, G. & Götz, M. Direct neuronal reprogramming: fast forward from new concepts toward therapeutic approaches. *Neuron* **110**, 366–393 (2022).
- Liu, Y. et al. CRISPR activation screens systematically identify factors that drive neuronal fate and reprogramming. *Cell Stem Cell* **23**, 758–771.e8 (2018).
- Masserdotti, G. et al. Transcriptional mechanisms of proneural factors and REST in regulating neuronal reprogramming of astrocytes. *Cell Stem Cell* **17**, 74–88 (2015).
- Vierbuchen, T. et al. Direct conversion of fibroblasts to functional neurons by defined factors. *Nature* **463**, 1035–1041 (2010).
- Zhang, Y. et al. Rapid single-step induction of functional neurons from human pluripotent stem cells. *Neuron* **78**, 785–798 (2013).
- Parras, C. M. et al. Divergent functions of the proneural genes *Mash1* and *Ngn2* in the specification of neuronal subtype identity. *Genes Dev.* **16**, 324–338 (2002).
- Yang, N. et al. Generation of pure GABAergic neurons by transcription factor programming. *Nat. Methods* **14**, 621–628 (2017).
- Velasco, S. et al. A multi-step transcriptional and chromatin state cascade underlies motor neuron programming from embryonic stem cells. *Cell Stem Cell* **20**, 205–217.e8 (2017).
- Franzén, O., Gan, L.-M. & Björkegren, J. L. M. PanglaoDB: a web server for exploration of mouse and human single-cell RNA sequencing data. *Database* **2019**, baz046 (2019).

33. Knöfler, M. et al. Human placenta and trophoblast development: key molecular mechanisms and model systems. *Cell. Mol. Life Sci.* **76**, 3479–3496 (2019).
34. Casey, B. H., Kollipara, R. K., Pozo, K. & Johnson, J. E. Intrinsic DNA binding properties demonstrated for lineage-specifying basic helix-loop-helix transcription factors. *Genome Res.* **28**, 484–496 (2018).
35. Guillemot, F., Nagy, A., Auerbach, A., Rossant, J. & Joyner, A. L. Essential role of Mash-2 in extraembryonic development. *Nature* **371**, 333–336 (1994).
36. Hughes, M. et al. The Hand1, Stra13 and Gcm1 transcription factors override FGF signaling to promote terminal differentiation of trophoblast stem cells. *Dev. Biol.* **271**, 26–37 (2004).
37. Kinoshita, M. et al. Disabling de novo DNA methylation in embryonic stem cells allows an illegitimate fate trajectory. *Proc. Natl Acad. Sci. USA* **118**, e2109475118 (2021).
38. Nehme, R. et al. Combining NGN2 programming with developmental patterning generates human excitatory neurons with NMDAR-mediated synaptic transmission. *Cell Rep.* **23**, 2509–2523 (2018).
39. Hitoshi, S. et al. Notch pathway molecules are essential for the maintenance, but not the generation, of mammalian neural stem cells. *Genes Dev.* **16**, 846–858 (2002).
40. Pierfelice, T., Alberi, L. & Gaiano, N. Notch in the vertebrate nervous system: an old dog with new tricks. *Neuron* **69**, 840–855 (2011).
41. Tian, R. et al. CRISPR interference-based platform for multimodal genetic screens in human iPSC-derived. *Neurons* **104**, 239–255.e12 (2019).
42. Tracey, T. J., Steyn, F. J., Wolvetang, E. J. & Ngo, S. T. Neuronal lipid metabolism: multiple pathways driving functional outcomes in health and disease. *Front. Mol. Neurosci.* **11**, 10 (2018).
43. Hulme, A. J., Maksour, S., St-Clair Glover, M., Mielliet, S. & Dottori, M. Making neurons, made easy: the use of Neurogenin-2 in neuronal differentiation. *Stem Cell Rep.* **17**, 14–34 (2022).
44. Michlits, G. et al. CRISPR-UML: single-cell lineage tracing of pooled CRISPR-Cas9 screens. *Nat. Methods* **14**, 1191–1197 (2017).
45. Hart, T. et al. High-resolution CRISPR screens reveal fitness genes and genotype-specific cancer liabilities. *Cell* **163**, 1515–1526 (2015).
46. Gascón, S. et al. Identification and successful negotiation of a metabolic checkpoint in direct neuronal reprogramming. *Cell Stem Cell* **18**, 396–409 (2016).
47. Russo, G. L. et al. CRISPR-mediated induction of neuron-enriched mitochondrial proteins boosts direct glia-to-neuron conversion. *Cell Stem Cell* **28**, 524–534.e7 (2021).
48. Cole, M. F., Johnstone, S. E., Newman, J. J., Kagey, M. H. & Young, R. A. Tcf3 is an integral component of the core regulatory circuitry of embryonic stem cells. *Genes Dev.* **22**, 746–755 (2008).
49. Jin, L. et al. Serine threonine kinase receptor-associated protein deficiency impairs mouse embryonic stem cells lineage commitment through CYP26A1-mediated retinoic acid homeostasis. *Stem Cells* **36**, 1368–1379 (2018).
50. Kielman, M. F. et al. Apc modulates embryonic stem-cell differentiation by controlling the dosage of β -catenin signaling. *Nat. Genet.* **32**, 594–605 (2002).
51. Quan, Y. et al. Cnot8 eliminates naïve regulation networks and is essential for naïve-to-formative pluripotency transition. *Nucleic Acids Res.* **50**, 4414–4435 (2022).
52. Wray, J. et al. Inhibition of glycogen synthase kinase-3 alleviates Tcf3 repression of the pluripotency network and increases embryonic stem cell resistance to differentiation. *Nat. Cell Biol.* **13**, 838–845 (2011).
53. Ying, Q.-L. et al. The ground state of embryonic stem cell self-renewal. *Nature* **453**, 519–523 (2008).
54. Zhang, Y., Ding, H., Wang, X. & Ye, S.-D. Modulation of STAT3 phosphorylation by PTPN2 inhibits naïve pluripotency of embryonic stem cells. *FEBS Lett.* **592**, 2227–2237 (2018).
55. Dai, Q. et al. Cyclin K-containing kinase complexes maintain self-renewal in murine embryonic stem cells. *J. Biol. Chem.* **287**, 25344–25352 (2012).
56. Lei, T. et al. Cyclin K regulates prereplicative complex assembly to promote mammalian cell proliferation. *Nat. Commun.* **9**, 1876 (2018).
57. Dutto, I., Tillhon, M., Cazzalini, O., Stivala, L. A. & Prosperi, E. Biology of the cell cycle inhibitor p21CDKN1A: molecular mechanisms and relevance in chemical toxicology. *Arch. Toxicol.* **89**, 155–178 (2015).
58. Johnson, P. F. Molecular stop signs: regulation of cell-cycle arrest by C/EBP transcription factors. *J. Cell Sci.* **118**, 2545–2555 (2005).
59. Bates, L. E., Alves, M. R. P. & Silva, J. C. R. Auxin-degron system identifies immediate mechanisms of OCT4. *Stem Cell Rep.* **16**, 1818–1831 (2021).
60. Niwa, H., Miyazaki, J. & Smith, A. G. Quantitative expression of Oct-3/4 defines differentiation, dedifferentiation or self-renewal of ES cells. *Nat. Genet.* **24**, 372–376 (2000).
61. Hough, S. R., Clements, I., Welch, P. J. & Wiederholt, K. A. Differentiation of mouse embryonic stem cells after RNA interference-mediated silencing of OCT4 and Nanog. *Stem Cells* **24**, 1467–1475 (2006).
62. Mall, M. et al. Myt1l safeguards neuronal identity by actively repressing many non-neuronal fates. *Nature* **544**, 245–249 (2017).
63. Pereira, L., Yi, F. & Merrill, B. J. Repression of Nanog gene transcription by Tcf3 limits embryonic stem cell self-renewal. *Mol. Cell Biol.* **26**, 7479–7491 (2006).
64. Yi, F. et al. Opposing effects of Tcf3 and Tcf1 control Wnt stimulation of embryonic stem cell self-renewal. *Nat. Cell Biol.* **13**, 762–770 (2011).
65. Nishimura, K., Fukagawa, T., Takisawa, H., Kakimoto, T. & Kanemaki, M. An auxin-based degron system for the rapid depletion of proteins in nonplant cells. *Nat. Methods* **6**, 917–922 (2009).
66. Creff, J. & Besson, A. Functional versatility of the CDK inhibitor p57Kip2. *Front. Cell Dev. Biol.* **8**, 584590 (2020).
67. Li, N. et al. p57 suppresses the pluripotency and proliferation of mouse embryonic stem cells by positively regulating p53 activation. *Stem Cells Int.* **2021**, 1–13 (2021).
68. Cheloufi, S. et al. The histone chaperone CAF-1 safeguards somatic cell identity. *Nature* **528**, 218–224 (2015).
69. Soufi, A., Donahue, G. & Zaret, K. S. Facilitators and impediments of the pluripotency reprogramming factors' initial engagement with the genome. *Cell* **151**, 994–1004 (2012).
70. Lu, Y.-L. & Yoo, A. S. Mechanistic insights into MicroRNA-induced neuronal reprogramming of human adult fibroblasts. *Front. Neurosci.* **12**, 522 (2018).
71. Wapinski, O. L. et al. Rapid chromatin switch in the direct reprogramming of fibroblasts to neurons. *Cell Rep.* **20**, 3236–3247 (2017).
72. Marro, S. et al. Direct lineage conversion of terminally differentiated hepatocytes to functional neurons. *Cell Stem Cell* **9**, 374–382 (2011).
73. Colasante, G., Rubio, A., Massimino, L. & Broccoli, V. Direct neuronal reprogramming reveals unknown functions for known transcription factors. *Front. Neurosci.* **13**, 283 (2019).
74. Smith, D. K., Yang, J., Liu, M.-L. & Zhang, C.-L. Small molecules modulate chromatin accessibility to promote NEUROG2-mediated fibroblast-to-neuron reprogramming. *Stem Cell Rep.* **7**, 955–969 (2016).
75. Liu, M.-L. et al. Small molecules enable neurogenin 2 to efficiently convert human fibroblasts into cholinergic neurons. *Nat. Commun.* **4**, 2183 (2013).
76. Chanda, S. et al. Generation of induced neuronal cells by the single reprogramming factor ASCL1. *Stem Cell Rep.* **3**, 282–296 (2014).
77. Tsunemoto, R. et al. Diverse reprogramming codes for neuronal identity. *Nature* **557**, 375–380 (2018).

78. Michlits, G., Burkard, T. R., Novatchkova, M. & Elling, U. CRISPR-UMI step by step: a protocol for robust CRISPR screening. *Protoc. Exch.* <https://doi.org/10.1038/protex.2017.111> (2017).
79. Love, M. I., Huber, W. & Anders, S. Moderated estimation of fold change and dispersion for RNA-seq data with DESeq2. *Genome Biol.* **15**, 550 (2014).
80. Kuleshov, M. V. et al. Enrichr: a comprehensive gene set enrichment analysis web server 2016 update. *Nucleic Acids Res.* **44**, W90–W97 (2016).
81. Stark, R. & Brown, G. DiffBind: differential binding analysis of ChIP-seq peak data. Bioconductor. <http://bioconductor.org/packages/release/bioc/vignettes/DiffBind/inst/doc/DiffBind.pdf> (2011).
82. Li, W. et al. MAGECK enables robust identification of essential genes from genome-scale CRISPR/Cas9 knockout screens. *Genome Biol.* **15**, 554 (2014).

Acknowledgements

We thank the VBCF-NGS team (<https://www.vbcf.ac.at>) for providing deep sequencing services and the IMBA-IMP BioOptics team for sharing expertise in flow cytometry, microscopy and cell sorting. We thank all the members of the Elling lab for their input and scientific discussions; Noelia Urban, Nicolas Rivron, and Bonkyoung Koo labs for sharing reagents; Dr. Torsten Reda and Dr. Mantas Survila for their expertise and LUTHOR 3'-scRNAseq library preparations.

Author contributions

U.E., M.W. and G.V. conceived and planned this project. G.V. designed and conducted experiments with the help of C.R., J.C.B. and J.L. G.V. performed data analysis with the help of M.N. and G.M. R.Y. provided expertise and helped with ChIP-seq experiments. M.W. provided initial cell lines for the experiments and valuable guidance throughout the project. U.E. supervised the project. G.V. and U.E. wrote the manuscript with input from all the co-authors.

Competing interests

The authors declare no competing interests.

Additional information

Supplementary information The online version contains supplementary material available at <https://doi.org/10.1038/s41467-023-40803-y>.

Correspondence and requests for materials should be addressed to Gintautas Vainorius or Ulrich Elling.

Peer review information *Nature Communications* thanks Raul Bressan and the other anonymous reviewer(s) for their contribution to the peer review of this work.

Reprints and permissions information is available at <http://www.nature.com/reprints>

Publisher's note Springer Nature remains neutral with regard to jurisdictional claims in published maps and institutional affiliations.

Open Access This article is licensed under a Creative Commons Attribution 4.0 International License, which permits use, sharing, adaptation, distribution and reproduction in any medium or format, as long as you give appropriate credit to the original author(s) and the source, provide a link to the Creative Commons license, and indicate if changes were made. The images or other third party material in this article are included in the article's Creative Commons license, unless indicated otherwise in a credit line to the material. If material is not included in the article's Creative Commons license and your intended use is not permitted by statutory regulation or exceeds the permitted use, you will need to obtain permission directly from the copyright holder. To view a copy of this license, visit <http://creativecommons.org/licenses/by/4.0/>.

© The Author(s) 2023